Etiology of distinct membrane excitability in pre- and posthearing auditory neurons relies on activity of Cl^- channel TMEM16A

Xiao-Dong Zhang[a], Jeong-Han Lee[b], Ping Lv[b,c], Wei Chun Chen[b], Hyo Jeong Kim[b], Dongguang Wei[b], Wenying Wang[b], Choong-Ryoul Sihn[b], Karen Jo Doyle[b], Jason R. Rock[d], Nipavan Chiamvimonvat[a,e], and Ebenezer N. Yamoah[b,1]

[a]Department of Internal Medicine, Division of Cardiovascular Medicine, School of Medicine, University of California, Davis, CA 95616; [b]Program in Communication Science, Department of Physiology, School of Medicine, University of Nevada, Reno, Reno NV 89557; [c]Department of Pharmacology, Hebei Medical University, Shijiazhuang 050017, China; [d]Department of Anatomy, School of Medicine, University of California, San Francisco, CA 94143; and [e]Department of Veterans Affairs, Northern California Health Care System, Mather, CA 95655

Edited by Richard W. Aldrich, The University of Texas at Austin, Austin, TX, and approved January 15, 2015 (received for review August 1, 2014)

The developmental rehearsal for the debut of hearing is marked by massive changes in the membrane properties of hair cells (HCs) and spiral ganglion neurons (SGNs). Whereas the underlying mechanisms for the developing HC transition to mature stage are understood in detail, the maturation of SGNs from hyperexcitable prehearing to quiescent posthearing neurons with broad dynamic range is unknown. Here, we demonstrated using pharmacological approaches, caged-Ca^{2+} photolysis, and gramicidin patch recordings that the prehearing SGN uses Ca^{2+}-activated Cl^- conductance to depolarize the resting membrane potential and to prime the neurons in a hyperexcitable state. Immunostaining of the cochlea preparation revealed the identity and expression of the Ca^{2+}-activated Cl^- channel transmembrane member 16A (TMEM16A) in SGNs. Moreover, null deletion of *TMEM16A* reduced the Ca^{2+}-activated Cl^- currents and action potential firing in SGNs. To determine whether Cl^- ions and TMEM16A are involved in the transition between pre- and posthearing features of SGNs we measured the intracellular Cl^- concentration $[Cl^-]_i$ in SGNs. Surprisingly, $[Cl^-]_i$ in SGNs from prehearing mice was ∼90 mM, which was significantly higher than posthearing neurons, ∼20 mM, demonstrating discernible altered roles of Cl^- channels in the developing neuron. The switch in $[Cl^-]_i$ stems from delayed expression of the development of intracellular Cl^- regulating mechanisms. Because the Cl^- channel is the only active ion-selective conductance with a reversal potential that lies within the dynamic range of SGN action potentials, developmental alteration of $[Cl^-]_i$, and hence the equilibrium potential for Cl^- (E_{Cl}), transforms pre- to posthearing phenotype.

hearing | spiral ganglion neurons | action potentials | calcium-activated chloride channels | development

The dynamic range of neuronal action potentials (APs) resides within voltages that are outside the reversal potentials (E_{rev}) of most ion currents except Cl^- currents, making Cl^- conductance the most versatile one in a course of a single AP. Neurons use this adaptable feature of Cl^- conductance with respect to the resting membrane potential (RMP) of neurons to confer synaptic plasticity by altering intracellular Cl^- (Cl^-_i) homeostasis during development. This process transforms depolarizing GABA/glycinergic-mediated responses in immature to hyperpolarizing responses in mature neurons (1, 2). A similar synaptic switch has been described in auditory brainstem neurons, where the mature GABA/glycinergic-induced inhibitory neurotransmission contributes strongly toward the computation of interaural level and time differences required for sound source localization (3–6). The depolarization mediated by GABA/glycine in early postnatal development may increase intracellular Ca^{2+} concentration ($[Ca^{2+}]_i$), which is predicted to promote synapse stabilization in the CNS (1). We hypothesized that besides synaptic plasticity one mechanism that alters the firing phenotype of developing neurons is via changes in intracellular Cl^- concentration ($[Cl]_i$) and activation of voltage and Ca^{2+}-activated Cl^- channels (CaCCs).

CaCCs are encoded by anoctamin 1 and 2 (*ANO1* and *2*), also known as transmembrane member 16A and B (*TMEM16A and B*) genes, which are expressed in epithelia and smooth muscle cells (7, 8) and in sensory cells such as nociceptive dorsal root ganglion neurons (9, 10), cilia of olfactory cells (11), and in rods and cones (12). The prevailing functions of CaCCs are ascribed to the amplification of pain sensation (10), cone responses (12), and olfactory signal transduction (13, 14), although recent reports using *TMEM16B* knockout mice suggest that CaCCs may play a limited role in signal amplification of olfactory transduction (11). TMEM16A has been identified in the cochlea in a cell-type-specific manner, showing robust labeling in basal cells of the stria vascularis and efferent endings of the auditory nerve (15), but its role in the inner ear has not been determined.

The trademark of the developing auditory neuron is the rhythmic and burst-patterned spontaneous AP (SAP), which is thought to shape synapse formation and refinement in the brainstem (16, 17). In the inner ear, inputs from Ca^{2+}-mediated SAPs from developing hair cells (HCs) sculpt the firing patterns of spiral ganglion neurons (SGNs) (18, 19). However, SGNs evolve from depolarizing hyperexcitable to hyperpolarized mature

Significance

One of the major issues in auditory neuroscience is the mechanism by which the developing hair cells and spiral ganglion neurons (SGNs) transition from prehearing characteristics to posthearing features. For decades it was thought that spontaneous action potentials in SGNs emanate from spontaneously firing prehearing hair cells. Here, we demonstrate that developing SGNs use Ca^{2+}-activated Cl^- conductance to depolarize the resting membrane potential and to prime the neurons in a hyperexcitable prehearing state. Moreover, SGNs undergo global changes in intracellular Cl^- homeostasis to alter their coding properties during development. Our findings address the endogenous origin of spontaneous activity in SGNs, transcend auditory-neuron-specific phenomena, and could open the flood gate for investigation on the mechanisms of Cl^- regulation in systems neuroscience.

Author contributions: X.-D.Z., J.-H.L., P.L., N.C., and E.N.Y. designed research; X.-D.Z., J.-H.L., P.L., W.C.C., H.J.K., D.W., W.W., C.-R.S., N.C., and E.N.Y. performed research; K.J.D., J.R.R., N.C., and E.N.Y. contributed new reagents/analytic tools; X.-D.Z., J.-H.L., P.L., W.C.C., H.J.K., C.-R.S., and K.J.D. analyzed data; and X.-D.Z., N.C., and E.N.Y. wrote the paper.

The authors declare no conflict of interest.

This article is a PNAS Direct Submission.

[1]To whom correspondence should be addressed. Email: enyamoah@gmail.com.

This article contains supporting information online at www.pnas.org/lookup/suppl/doi:10.1073/pnas.1414741112/-/DCSupplemental.

neurons with a wide dynamic range (20). Mechanisms underlying the remarkable changes in SGN phenotype during development are not well understood. Here, we demonstrate the origin and molecular mechanisms of the transition from primordial to mature auditory neurons. SGNs undergo marked alterations in intracellular Cl^- concentration ($[Cl^-]_i$) handling during development and in doing so transform a predominantly inwardly driven Cl^- current into outwardly directed current through activation of TMEM16 channels.

Results

SGNs were isolated from the cochlea of prehearing [postnatal day (P) 1 or 2] and posthearing (1- to 2-mo-old) male and female mice. SGNs were maintained in culture for 1–2 d to allow Schwann cells from neuronal membrane surfaces to detach.

Developmental Changes in AP Phenotype from Pre- to Posthearing SGNs. Previous reports have shown that developing auditory nerves discharge waves of SAPs that were thought to originate from SAPs of primordial HCs (17, 18). Although these patterned activities from HCs may represent the basis of synaptic plasticity in the developing cochlear nuclei (3), we and others have demonstrated that developing SGNs exhibit intrinsic conductances that generate SAPs (21). Shown in Fig. 1*A* are SAP firings recorded from P2–P56 SGNs. Noticeably, the RMPs in pre- and posthearing neurons were distinct (prehearing, -56 ± 7 mV; $n = 18$; posthearing, -64 ± 5 mV; $n = 24$; $P < 0.01$). Spontaneously active neurons in the basal and apical turns of the cochlea in prehearing were approximately threefold greater than posthearing neurons (Fig. 1 *A* and *D*). We reasoned that a Cl^- conductance may be an important contributor to the SAP firing of SGNs.

Inhibitors of Cl^- Channels Hyperpolarize the Cell Membrane and Reduce AP Firing of SGNs. We applied Cl^- channel inhibitors to examine the possible roles of the Cl^- conductance in SGNs. Suppression of Cl^- conductance with 100 μM niflumic acid (NFA) significantly reduced the firing of SAPs and evoked APs. The inhibitory effect was reversible after washout (Fig. 1 *B* and *C*). As shown in Fig. 1*B*, *Middle* and *Right*, 100 μM NFA and another Cl^- channel blocker, 5-nitro-2-(3-phenylpropylamino) benzoic acid (NPPB), significantly hyperpolarized the RMPs in P2 neurons [control: -58 ± 4 mV, NFA: -63 ± 3 mV ($n = 9$, $P < 0.01$); control: -59 ± 3 mV, NPPB: -66 ± 5 mV ($n = 8$, $P < 0.01$)] and eliminated or reduced the evoked AP firing in P2 SGNs (Fig. 1 *C* and *D*). In contrast, NFA and NPPB produced moderate effects on the RMPs of P56 neurons [control: -62 ± 2 mV, NFA: -65 ± 2 mV ($n = 7$, $P < 0.05$); control: -64 ± 2 mV, NPPB: -67 ± 3 mV ($n = 8$, $P < 0.05$)]. The reversible effect of the two Cl^- channel blockers further provides evidence that Cl^- conductance regulates the excitability of SGNs.

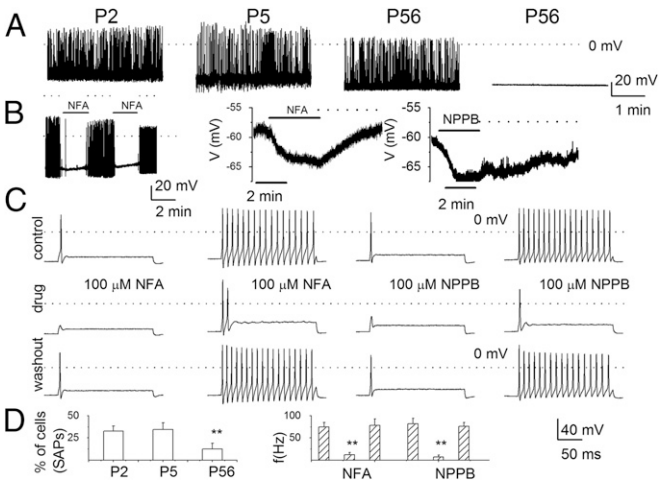

Fig. 1. Inhibitors of chloride channels hyperpolarized the RMP and reduced the AP firings in SGNs. (*A*) SAP firing of prehearing SGNs at P2 and P5 (two left panels). For posthearing neurons at P56, there were neurons with SAPs and others without (two right panels). The percentages of cells exhibiting SAPs are summarized in *D*, *Left* [P2 ($n = 156$), P5 ($n = 101$), and P56 ($n = 96$)]. The dashed lines represent 0 mV. (*B*) SAP firings of SGNs recorded from P2 neurons were attenuated upon application of 100 μM NFA (solid line) and the effect was reversible after washout (dotted line) (*Left*). For quiescent neurons, 100 μM NFA (*Middle*) or NPPB (*Right*) reversibly mediated membrane hyperpolarization. (*C*) NFA and NPPB significantly attenuated evoked APs recorded in P2 neurons. The dashed lines represent 0 mV. The summary data are shown in *D*, *Right*. In contrast to P2 neurons, the effects of NFA on P56 neurons were less apparent. Controls: 64 ± 12 Hz; NFA, 48 ± 18 Hz ($n = 5$, $P < 0.137$, not statistically significant).

Ca^{2+}-Activated Cl^- Channels in SGNs. The Cl^- conductance in SGNs could stem from one or several subtypes of Cl^- channels including voltage-gated, volume-regulated, ligand-gated, and Ca^{2+}-activated Cl^- channels (22). Among these candidates, TMEM16A, a member of CaCCs, has been localized in nerve terminals of SGNs (15). This is further supported by the expression of the TMEM16 protein in the cell body and neurites of primary cultures of SGNs (Figs. S1 and S2). CaCCs could be activated by Ca^{2+} influx through voltage-gated Ca^{2+} channels or Ca^{2+} signaling via inositol trisphosphate receptors (10). To directly test the possible roles of CaCCs in SGNs, we recorded the RMPs and AP firings before and after the release of caged Ca^{2+}. Indeed, UV photolysis of caged Ca^{2+} depolarized the RMPs and enhanced AP firing significantly (Fig. S3). The effects of caged-Ca^{2+} release were more pronounced in P2 SGNs compared with adult neurons (P56) as assessed by alterations of the RMPs (Fig. S3*B*) and the firing frequency of AP (Fig. S3*D*).

To further address the functional role of CaCCs in SGNs, we directly recorded the Ca^{2+}-activated Cl^- currents in SGNs by using caged-Ca^{2+} photolysis under conditions where only Cl^- conductance could be assessed (*Materials and Methods*). Fig. 2*A* shows a typical Ca^{2+}-activated Cl^- current trace recorded from SGNs after UV photolysis. To characterize the currents, we varied the UV-exposure time to record the time-dependent activation of the currents as shown in Fig. 2*B*. There was a positive correlation between the UV-exposure time and the current amplitude, which approached saturation beyond 700 ms. The UV-exposure time-dependent activation of the Ca^{2+}-activated Cl^- currents is shown in Fig. 2*C* with a half-activation time of ~300 ms. To address features of the Ca^{2+}-activated current, we used a dual-ramp pulse to measure the activation and the current–voltage relationship in SGNs as shown in Fig. 2*D*. The voltage ramp ranged from −80 to 80 mV for 4 s. The first voltage ramp was applied in the absence of UV and the second ramp was applied in the presence UV light as indicated (red bar in Fig. 2*D*). The activation time course of the current is shown as an inset with a time constant (τ) of 608 ± 108 ms ($n = 6$). The difference current, generated by subtracting currents under the two different conditions, was considered as the bona fide Ca^{2+}-activated Cl^- currents (Fig. 2*E*). The estimated equilibrium potential of the Cl^- currents (E_{Cl}) under the recording condition at room temperature is ~−38 mV. The measured reversal potential for the difference current (E_{rev}) was -30 ± 3 mV ($n = 8$), supporting the notion that the current is likely carried by Cl^- ions. Next, we estimated the Cl^- conductance in SGNs. From Fig. 2*A*, using a peak current of ~150 pA, the Ca^{2+}-activated Cl^- conductance was ~1.5 nS for the P56 neuron.

We further examined the expression of TMEM16A and B in mouse cochlea sections of P1, P14 (2 wk), and P28 (4 wk) mice. Antibodies directed against TMEM16A and 16B showed positive reactivity in SGNs, suggesting that both TMEM16A and 16B are expressed in SGNs (Fig. 3).

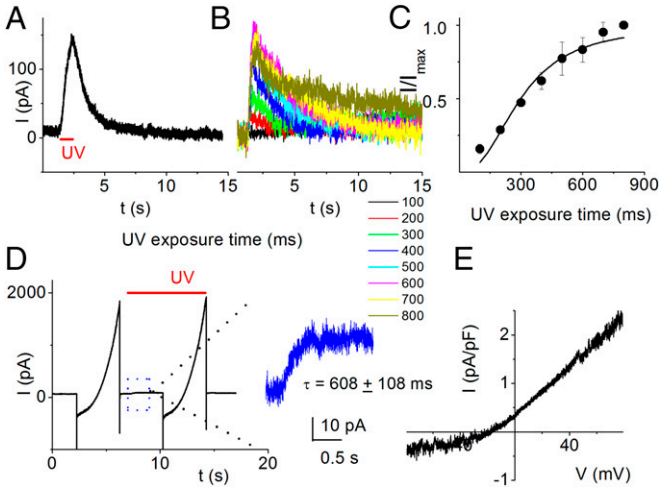

Fig. 2. Identification of Ca^{2+}-activated Cl^- currents in SGNs. Whole-cell recordings were performed in primary cultures of SGNs. Neurons were loaded with caged Ca^{2+} and Ca^{2+} was released using UV photolysis. (*A*) Ca^{2+}-activated Cl^- currents in SGNs elicited by UV photolysis at 60 mV. (*B*) UV exposure time was varied between 100–800 ms to activate the currents. (*C*) Summary data of the exposure time-dependent activation of the outward currents. Currents were normalized to the peak current induced by exposure time of 800 ms ($n = 4$ cells). (*D*) A dual ramp protocol from −80 to +80 mV was applied before and after UV application from a holding potential of 0 mV. The inset in blue trace shows the activation time course of the Ca^{2+}-activated Cl^- channel by UV light ($\tau = 608 \pm 108$ ms when fitted with a single exponential function; $n = 6$ cells). (*E*) Current–voltage relationship of the difference current. The difference current obtained before and after UV application was considered to be Ca^{2+}-activated Cl^- currents.

Reduced Ca^{2+}-Activated Cl^- Currents and Altered AP Firing in SGNs from TMEM16A Knockout (*TMEM16A*$^{-/-}$) Mice. To examine the contribution of TMEM16A to the Ca^{2+}-activated Cl^- currents in SGNs, we tested *TMEM16A*$^{-/-}$ mice. Indeed, the Ca^{2+}-activated Cl^- currents were substantially reduced in SGNs from *TMEM16A*$^{-/-}$ mice compared with WT littermates (Fig. S4*A*). In support of the evidence that the Ca^{2+}-activated Cl^- current contributes substantially toward the prehearing SAPs and increased excitability of the developing SGNs, we observed attenuated SAPs and hyperpolarized RMP in prehearing *TMEM16A*$^{-/-}$ SGNs (P11). The mean RMP for P11 SGNs isolated from *TMEM16A*$^{-/-}$ was -62 ± 5 mV ($n = 15$) compared with their WT littermate neurons (-54 ± 4 mV; $n = 14$; $P < 0.01$). Additionally, among the 72 neurons that were sampled from the *TMEM16A*$^{-/-}$ mice, only two (~3%) were spontaneously active compared with ~33% in control neurons. Furthermore, the inhibitory effects mediated by 100 μM NFA on AP firing of SGNs from *TMEM16A*$^{-/-}$ mice were significantly reduced compared with those of WT SGNs, as shown in Fig. S4 *B* and *C*. For example, for fast-adapting neurons that elicited a single spike after 200-ms current (0.2 nA) injection (Fig. S4*B*), NFA had no significant effect on *TMEM16A*$^{-/-}$ SGN AP firing (neuron spike frequency before NFA: 5 ± 0 Hz, after NFA: 5 ± 0 Hz, $n = 17$, not statistically significant). Similarly, in another set of neurons, whose response to current injection was slowly adapting (Fig. S4*C*), NFA did not significantly alter the firing frequency of the neurons (before NFA: 25 ± 7 Hz, after NFA: 16 ± 11 Hz, $n = 9$, not statistically significant). We were unable to evaluate the properties of *TMEM16A*$^{-/-}$ SGNs in older mice because all null mutation mice died before P21.

Changes in $[Cl^-]_i$ in SGNs from Pre- to Posthearing SGNs. We hypothesized that developmental alterations in $[Cl^-]_i$ and the corresponding changes in E_{Cl} may serve as one of the mechanisms underlying the differences in membrane excitability between pre- and posthearing SGNs. We determined E_{Cl} in pre-hearing (P2) and posthearing (P56) neurons as an indirect strategy to estimate the $[Cl^-]_i$ using gramicidin perforated patches, which have been demonstrated to preserve $[Cl^-]_i$ (23). These analyses suggested that the $[Cl^-]_i$ were high in prehearing neurons (~90 mM) but plummeted in posthearing SGNs (~20 mM) (Fig. 4 *A*–*C*).

To further corroborate the findings from gramicidin experiments, we measured $[Cl^-]_i$ directly using a Cl^- fluorescence dye, N-(ethoxycarbonylmethyl)-6-methoxyquinolinium bromide (MQAE) (Life Technologies). Fig. 4 *D* and *F* show fluorescence intensities measured in P2 and P56 SGNs when cells were challenged by Tyrode's solution and the calibration solutions with four different chloride concentrations ($[Cl^-]$). In situ calibrations were performed using solutions with different $[Cl^-]$ and two ionophores, the Cl^-/OH^- antiporter tributyltin and K^+/H^+ antiporter negericin. To account for the quenching effects of the MQAE fluorescence signals by the increased $[Cl^-]$, we normalized the fluorescence intensities to the maximum intensity at 0 mM $[Cl^-]_i$. The Stern–Volmer equation was used to calculate the $[Cl^-]_i$ in SGNs based on the measurement in Tyrode's solution (Fig. 4 *E* and *G*). The summary data are shown in Fig. 4*H*. The $[Cl^-]_i$ in P2 SGNs was two- to threefold higher than that from the adult mice. However, there was no significant difference in $[Cl^-]_i$ between apical and basal SGNs in pre- and posthearing mice (Fig. 4*H*). To ensure the reliability of $[Cl^-]_i$ measurements, we recorded the MQAE signal for more than 200 s in SGNs to rule out the bleaching effects of the fluorescence signal (Fig. 4*I*).

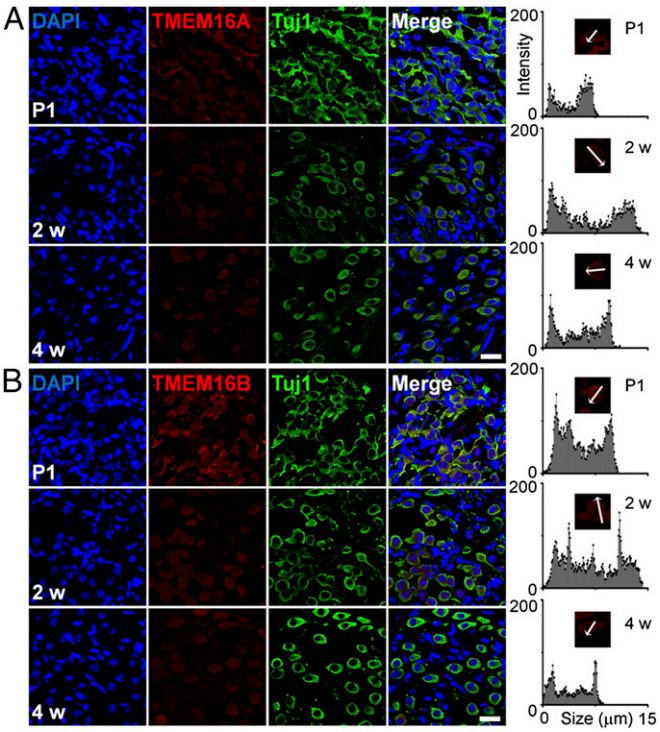

Fig. 3. Expression of TMEM16A and TMEM16B in SGNs (*A*) Expression of TMEM16A in SGNs from mice at P1, P14 (2 wk), and P28 (4 wk) as indicated. Neurons were labeled with the neuronal marker Tuj1 (cyan). TMEM16A was labeled in red and the nuclei were stained with DAPI (blue). Merged images are shown on the right. (*B*) Expression of TMEM16B in SGNs from the same age group as in *A*. The observations were made in 30 slides from three mice of P1 (30/3 for P1), 40/3 for 2 wk, and 40/3 for 4 wk. (Scale bars, 10 μm.)

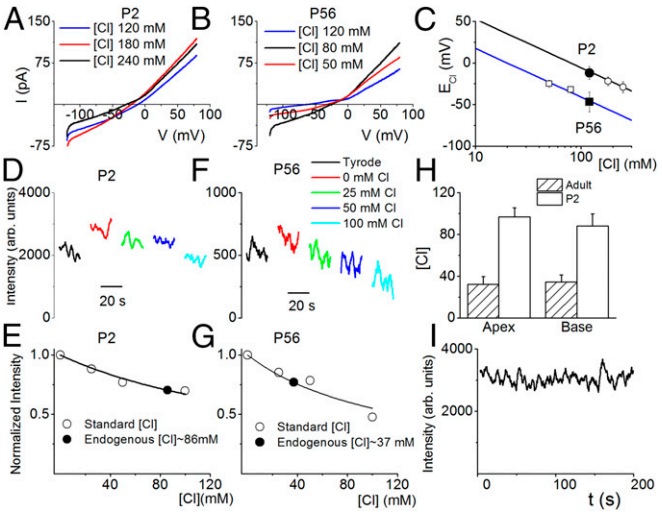

Fig. 4. Intracellular Cl^- concentrations ($[Cl^-]_i$) of spiral ganglion neurons from prehearing (P2) and posthearing (P56) mice. (*A* and *B*) Ramp protocol elicited NFA-sensitive currents recorded using gramicidin perforated patches from P2 (*A*) and P56 (*B*). We used the recorded reversal potential (e.g., ∼−11 mV) (in blue) as shown for a P2 neuron (*A*) and ∼−60 mV (in blue) for a P56 neuron (*B*) to estimate the $[Cl^-]_i$. To ascertain that we were indeed recording the activity of Cl^- conductance, we altered the external $[Cl^-]$ as indicated. The E_{Cl} changed in the expected direction. (*C*) Line graph depicting the calculated E_{Cl} versus external $[Cl^-]$. The solid symbols shows the estimated E_{Cl} that was used to calculate $[Cl^-]_i$ in P2 (circle) and P56 (square) neurons. Data assembled from P2 and P56 neurons suggested that $[Cl^-]_i$ were; 86 ± 8 mM (n = 11) and 18 ± 5 mM (n = 9), respectively. The open symbols represented the measured E_{Cl} upon bath perfusion of different external $[Cl^-]$. (*D* and *F*). The fluorescence intensity of MQAE measured in P2 (*D*) and P56 (*F*) SGNs. In situ calibrations were conducted by using four standard solutions containing 0, 25, 50, and 100 mM Cl^- following the measurement in Tyrode's solution for each cell. (*E* and *G*). The Stern–Volmer equation was used to fit the calibration data (open circles) from the measurement in P2 (*E*) and P56 (*G*) SGNs as shown by the solid line. The fluorescence intensity was normalized by that measured in 0 mM Cl^- calibration solution. Fluorescence intensity measured in the Tyrode's solution was used to calculate the $[Cl^-]_i$ based on the parameters from the curve fitting. The closed circle represents the fluorescence intensity in Tyrode's solution. (*H*) Comparisons of the $[Cl^-]_i$ of SGNs between P2 and P56 SGNs. There was no significant difference in $[Cl^-]_i$ between apical and basal SGNs in neonatal and adult mice, but the $[Cl^-]_i$ in neonatal SGNs were approximately two- to threefold higher than that in adult SGNs (Adult/Apex: n = 4; Adult/Base: n = 8; P2/Apex: n = 8; P2/Base: n = 6). (*I*) Negligible bleaching effects of MQAE fluorescence signal. As a control, we recorded the emission of MQAE for more than 200 s in SGN to monitor the bleaching effects of the fluorescence signal and did not observe the significant bleaching.

Expression of Cl^- Regulatory Molecules in Pre- and Posthearing SGNs. Using antibodies specific for Na–K–Cl cotransporter 1 (NKCC1) and K–Cl cotransporter (KCC2) in cochlea sections, we demonstrated in Fig. 5 that the two proteins are expressed in the plasma membrane of SGNs (also see Fig. S5). However, longitudinal assessment (P1–P28) of the expression profile of the two proteins shows that they are expressed later in development, raising the possibility that developmental regulatory mechanisms of $[Cl^-]_i$ in SGNs may lag behind the activity of TMEM16 channels. Thus, a scheme whereby the E_{Cl} is altered during development may help to explain the differential excitability of pre- and posthearing neurons (Fig. 5*C*).

Discussion

CaCCs were first recorded in *Xenopus* oocytes (24). The developmental roles of CaCCs became immediately apparent when it was demonstrated that fertilization-mediated Ca^{2+} inflow activated CaCCs to induce membrane depolarization, impairing additional sperm fusion and preventing triploidy (24). Subsequently, CaCCs have been identified and implicated in epithelial secretion (25); regulation of photo and olfactory transduction (11, 12, 26); and neuronal, cardiac, and smooth muscle function (27, 28). However, the molecular identity of CaCCs has only been reported recently (27, 29, 30). *TMEM16A* and its close paralogue *TMEM16B* have been demonstrated to encode for CaCCs (31), whereby in the presence of permissive $[Ca^{2+}]_i$ membrane depolarization enhances the current magnitude. The activity of the two proteins confers transepithelial anion transport and smooth muscle contraction, as well as amplifies olfactory signal transduction (28). Moreover, TMEM16A is overexpressed in several cancer cells and its suppression may mitigate their metastasis (32, 33). Recently, the expression of TMEM16A was identified in basal cells of the stria vascularis and efferent endings of the auditory nerve (15), but its functional role in the inner ear is not known.

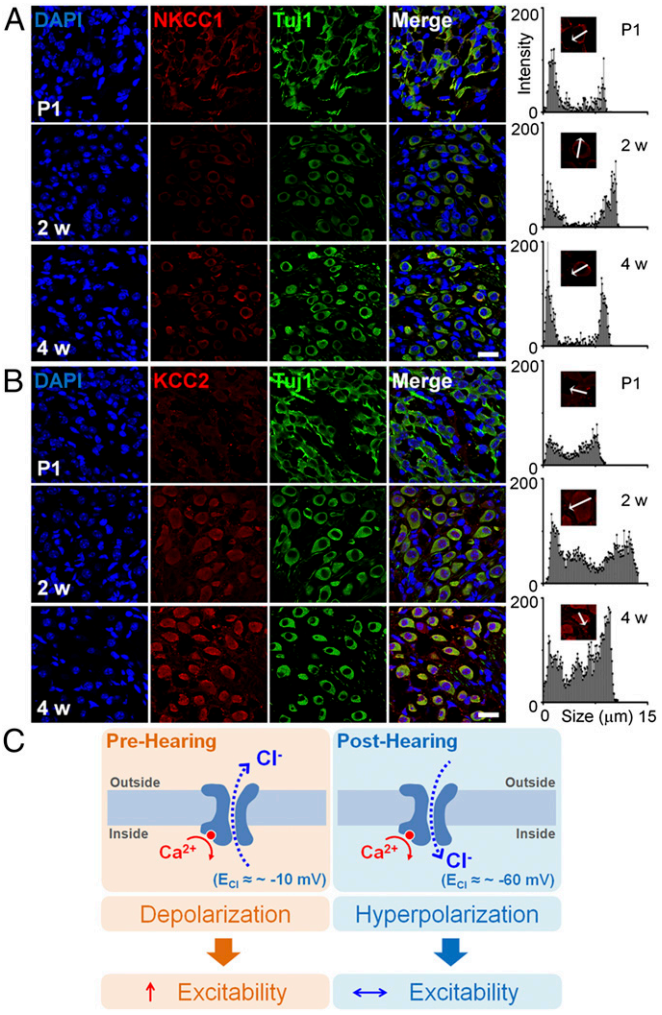

Fig. 5. NKCC1 and KCC2 expressions in SGNs. (*A*) Expression of NKCC1 in SGNs from mice of P1, P14 (2 wk), and P28 (4 wk) as indicated. Neurons were labeled with the neuronal marker Tuj1 (green). NKCC1 was labeled in red and the nuclei were stained with DAPI (blue). Merged images are shown on the right. (*B*) Expression of KCC2 in SGNs from similar age group as in *A*. The labeling follows similar order as described in *A*. The observations were made in 30 slides from 3 mice of P1 (30/3 for P1), 40/3 for 2 wk, and 40/3 for 4 wk. (Scale bars, 10 μm.) (*C*) Schematic representation of developmental changes in $[Cl^-]_i$ and the ensuing changes in the direction of Cl^- currents in neonatal and adult SGNs.

Here, we demonstrate that the transition of SGNs from developing to mature phenotype relies to a major extent on the activity of TMEM16. Pharmacological suppression of Cl^- currents in the developing SGNs attenuates SAPs, whereas in quiescent neurons inhibition of Cl^- currents promotes membrane hyperpolarization and reduces evoked spike activity. Because the activation of CaCCs can be mediated by $Ca^{2+}{}_i$ release and signaling (9, 10), we used caged-Ca^{2+} photolysis to demonstrate the CaCCs in SGNs. We then took advantage of a gene-targeted mouse model to document the role of TMEM16A as one of the molecular correlates of CaCCs in SGNs. The expression of TMEM16B in SGNs further raises the possibility that TMEM16A and 16B may form heteromeric channels. Cl^- current and evoked AP measurements from SGNs isolated from *TMEM16A*$^{-/-}$ mice support the functional contribution of TMEM16A to the excitability of SGNs. The importance of TMEM16A in SGNs is underpinned by the surprising revelation that $[Cl^-]_i$ is under dynamic regulation in the developing SGNs, ranging from ∼90 mM in prehearing SGNs to ∼20 mM in posthearing neurons. Thus, the expected shift in E_{Cl} transforms a seemingly depolarizing-mediated current to hyperpolarizing current with respect to the RMP of SGNs. The proposed developmental shift in E_{Cl} in SGNs may stem from delay in the expression and activity of Cl^- regulatory mechanisms including NKCC1 and KCC2. Even though the activation of the Cl^- conductance produces an inward current early in neuronal development, it may nevertheless reduce membrane excitability if its effect on membrane gain exceeds its effect on the net inward current. This possibility can be further addressed using a quantitative model.

Previous reports have used direct and indirect methods to estimate neuronal $[Cl^-]_i$. Depending on the developmental stages and different regions of the brain, $[Cl^-]_i$ ranges from ∼20–40 mM (34–36). Increased $[Cl^-]_i$ levels in neocortical (37), spinal cord (38), and cerebellar neurons (39) are considered transient and are features of immature neurons. Moreover, there are several evolutionarily conserved synaptic-response-switch mechanisms from GABA/glycine-mediated early depolarization and later hyperpolarization in mature stages. The time course of the $[Cl^-]_i$ regulation coincides with temporal changes in the expression and activity of Cl^- transport mechanisms as well as the depolarization-to-hyperpolarization synaptic transformation in specific brain nuclei (40). However, in other areas such as the spinal cord and hippocampus (41, 42) the developmental switch in synaptic responses from GABA/glycine-mediated depolarization to hyperpolarization is not consistent with the time course of the maturation of the Cl^- regulatory proteins, making it difficult to establish direct causal relations.

Besides nuclear and cell-specific global differences in Cl^- regulation in certain regions of the brain, there can be marked modifications in Cl^- handling within restricted domains in a given cell. Indeed, as demonstrated in the retina and suprachiasmatic nucleus (43, 44), the Cl^- handling may be delimited to different subcellular compartments, which will afford rapid and privileged synaptic signaling. Thus, it is conceivable that in the network of dendritic arbors a neuron may integrate depolarizing and hyperpolarizing signals, which is mediated by the same neurotransmitter in signal processing. Such finely tuned Cl^- homeostasis will require specialized Cl^- regulatory capabilities such as cation–chloride cotransporters (45).

In contrast to the CNS and the spinal cord, there are startling and profound differences in Cl^- handling in the auditory brainstem. Increased Cl^- accumulation is mediated by the activity of NKCC1 early in development, but it seems that the Cl^-/HCO_3^- exchanger AE3 (46) and other Cl^- transporters may operate in a cell-specific manner (47). Reduction of $[Cl^-]_i$ in mature neurons may rely on gradual down-regulation of NKCC1 (40). Further contrasting features of the chick auditory brainstem are the apparent maintenance of high $[Cl^-]_i$ and inwardly directed Cl^- current at the RMP even in adult neurons, conferring GABA-induced inhibition by way of activation of K_v1 subtype of channels to promote shunting inhibition (4). Although the nuances of Cl^- regulatory mechanism in auditory brainstem neurons are not fully understood and continue to evolve, it is clear that spatial Cl^- regulation in distinct subcellular compartments may yield multiple synaptic outputs from limited numbers of neurotransmitters.

Findings from the present study suggest that the developmental roles of CaCCs are not restricted solely to synaptic plasticity, but extend to activity-dependent membrane plasticity that shapes neuronal wiring. Evidently, inhibition or total removal and overstimulation of SGNs of the developing cochlea have profound impact on the number and size of auditory brainstem nuclei (48, 49). However, these previous studies do not distinguish between the contribution of intrinsically generated SAPs from hair cells or SGNs. New insights into the fundamental mechanisms underlying the transition from hyperexcitability in juvenile stage to adult phenotypes continue to evolve.

Materials and Methods

All animal care and procedures were performed in accordance with National Institutes of Health guidelines and were approved by the Institutional Animal Care and Use Committee of the University of California, Davis.

Isolation and Culture of SGNs. SGNs were isolated and maintained in culture as we have previously described (21). Immunofluorescence confocal microscopy of the cultured SGNs and cochlea sections was performed as previously described (21) and is presented in greater detail in *SI Materials and Methods*.

Intracellular Cl^- Concentration Measurements. We used MQAE fluorescent dye (Life Technologies) to measure the $[Cl^-]_i$ as previously described (50). The cultured adult (P56) or P2 SGNs were first loaded by incubating cells in Tyrode's solution containing 5 mM MQAE for 30 min at room temperature. The Tyrode's solution contained (in millimolar) 140 NaCl, 5.4 KCl, 1 $MgCl_2$, 2 $CaCl_2$, 10 glucose, and 10 Hepes, pH 7.4. The standard high-Cl^- solution contained (in millimolar) 150 KCl, 2 $CaCl_2$, 10 glucose, and 10 Hepes, pH 7.4. The reduced Cl^- solutions were made by substitution of KNO_3 for KCl in the standard high-Cl^- solution. Tributyltin (20 mM) and negericin (5 mM) in ethanol were stored at −20 °C. The two ionophores were diluted in the calibration solution immediately before use.

Patch-Clamp Recording. Patch-clamp recordings were performed using an Axopatch 200B amplifier, Digidata 1440A digitizer, and pClamp10 software (Molecular Devices).

For evoked AP recording, extracellular solution contained (in millimolar) 130 NaCl, 5 KCl, 1 $MgCl_2$, 2 $CaCl_2$, 10 D-glucose, and 10 Hepes, pH 7.3. The normal internal solution contained (in millimolar) 112 KCl, 1 $MgCl_2$, 0.01 $CaCl_2$, 5 ATP-K_2, and 10 Hepes, pH 7.35. For measurement of RMP, and evoked AP recordings using caged-Ca^{2+} photolysis, the internal solution contained (in millimolar) 112 KCl, 0.5 $CaCl_2$, 5 ATP-K_2, 20 Hepes, and 2 DMNP-EDTA (Life Technologies), pH 7.35.

For amphotericin perforated patch experiments, pipettes were filled with the internal solution containing (in millimolar) 150 KCl, 10 Hepes, and 10 D-glucose, pH 7.3. For gramicidin perforated patch experiments, extracellular solution contained (in millimolar) 109 NaCl, 5 KCl, 1 $MgCl_2$, 2 $CaCl_2$, 10 D-glucose, and 10 Hepes, pH 7.3. For the reduced extracellular Cl^- concentrations, NaCl was substituted for Na-gluconate, or Na-methanesulphonate. A stock solution of gramicidin (20 mg/mL) was made using DMSO. Pipettes were filled with the internal solution containing (in millimolar) 120 KCl, 10 Hepes, and 20–50 D-glucose, pH 7.3.

For whole-cell Ca^{2+}-activated chloride current recording by using UV photolysis, DMNP-EDTA was included in the pipette solution. The pipette solution contained (in millimolar) 30 CsCl, 110 Na-glutamate, 20 Hepes, 0.5 $CaCl_2$, and 2 DMNP-EDTA, pH 7.4. The external solution contained (in millimolar) 130 NaCl, 5 $MgCl_2$, 10 Hepes, and 1 EGTA, pH 7.4.

To minimize liquid junction potentials (LJPs), we used 3 M KCl agar bridges in all electrophysiological experiments. The LJPs were measured and corrected as described (51). The LPJs were as follows (in millivolts): NaCl, −2.8 ± 0.8 (n = 106); Na^+-gluconate, −4.6 ± 1.8 (n = 98); and Na^+-methanesulphonate, −5.2 ± 1.4 (n = 54). We also measured and corrected for the potential across the perforated patches [2.5 ± 1.4 (n = 78)]. See *SI Materials and Methods* for detailed solutions and recording configurations.

ACKNOWLEDGMENTS. This work was supported by National Institutes of Health (NIH)/National Institute on Deafness and Other Communication Disorders Grants R01DC003826 and DC010386 (to E.N.Y.), NIH/National Heart, Lung, and Blood Institute Grants R01HL085727 and R01HL085844 (to N.C.), Veterans Affairs Merit Review Grant I01BX000576 (to N.C.), and American Heart Association Western States Affiliate Beginning Grant-in-Aid 14BGIA18870087 (to X.-D.Z.).

1. Ben-Ari Y, Gaiarsa JL, Tyzio R, Khazipov R (2007) GABA: A pioneer transmitter that excites immature neurons and generates primitive oscillations. *Physiol Rev* 87(4): 1215–1284.
2. Titz S, et al. (2003) Hyperpolarizing inhibition develops without trophic support by GABA in cultured rat midbrain neurons. *J Physiol* 550(Pt 3):719–730.
3. Howard MA, Rubel EW (2010) Dynamic spike thresholds during synaptic integration preserve and enhance temporal response properties in the avian cochlear nucleus. *J Neurosci* 30(36):12063–12074.
4. Kuo SP, Bradley LA, Trussell LO (2009) Heterogeneous kinetics and pharmacology of synaptic inhibition in the chick auditory brainstem. *J Neurosci* 29(30):9625–9634.
5. Milenković I, et al. (2007) Development of chloride-mediated inhibition in neurons of the anteroventral cochlear nucleus of gerbil (Meriones unguiculatus). *J Neurophysiol* 98(3):1634–1644.
6. Kandler K, Friauf E (1995) Development of glycinergic and glutamatergic synaptic transmission in the auditory brainstem of perinatal rats. *J Neurosci* 15(10):6890–6904.
7. Huang F, et al. (2009) Studies on expression and function of the TMEM16A calcium-activated chloride channel. *Proc Natl Acad Sci USA* 106(50):21413–21418.
8. Manoury B, Tamuleviciute A, Tammaro P (2010) TMEM16A/anoctamin 1 protein mediates calcium-activated chloride currents in pulmonary arterial smooth muscle cells. *J Physiol* 588(Pt 13):2305–2314.
9. Liu B, et al. (2010) The acute nociceptive signals induced by bradykinin in rat sensory neurons are mediated by inhibition of M-type K+ channels and activation of Ca2+-activated Cl- channels. *J Clin Invest* 120(4):1240–1252.
10. Jin X, et al. (2013) Activation of the Cl- channel ANO1 by localized calcium signals in nociceptive sensory neurons requires coupling with the IP3 receptor. *Sci Signal* 6(290): ra73.
11. Billig GM, Pál B, Fidzinski P, Jentsch TJ (2011) Ca2+-activated Cl− currents are dispensable for olfaction. *Nat Neurosci* 14(6):763–769.
12. Barnes S, Hille B (1989) Ionic channels of the inner segment of tiger salamander cone photoreceptors. *J Gen Physiol* 94(4):719–743.
13. Kurahashi T, Yau KW (1993) Co-existence of cationic and chloride components in odorant-induced current of vertebrate olfactory receptor cells. *Nature* 363(6424): 71–74.
14. Reisert J, Lai J, Yau KW, Bradley J (2005) Mechanism of the excitatory Cl- response in mouse olfactory receptor neurons. *Neuron* 45(4):553–561.
15. Jeon JH, et al. (2011) Expression and immunohistochemical localization of TMEM16A/anoctamin 1, a calcium-activated chloride channel in the mouse cochlea. *Cell Tissue Res* 345(2):223–230.
16. Jones TA, Jones SM (2000) Spontaneous activity in the statoacoustic ganglion of the chicken embryo. *J Neurophysiol* 83(3):1452–1468.
17. Jones TA, Jones SM, Paggett KC (2001) Primordial rhythmic bursting in embryonic cochlear ganglion cells. *J Neurosci* 21(20):8129–8135.
18. Tritsch NX, et al. (2010) Calcium action potentials in hair cells pattern auditory neuron activity before hearing onset. *Nat Neurosci* 13(9):1050–1052.
19. Levic S, et al. (2007) Development and regeneration of hair cells share common functional features. *Proc Natl Acad Sci USA* 104(48):19108–19113.
20. Lv P, Wei D, Yamoah EN (2010) Kv7-type channel currents in spiral ganglion neurons: involvement in sensorineural hearing loss. *J Biol Chem* 285(45):34699–34707.
21. Lv P, et al. (2012) Posthearing Ca(2+) currents and their roles in shaping the different modes of firing of spiral ganglion neurons. *J Neurosci* 32(46):16314–16330.
22. Ferrera L, Zegarra-Moran O, Galietta LJ (2011) Ca2+-activated Cl- channels. *Compr Physiol* 1(4):2155–2174.
23. Kyrozis A, Reichling DB (1995) Perforated-patch recording with gramicidin avoids artifactual changes in intracellular chloride concentration. *J Neurosci Methods* 57(1): 27–35.
24. Miledi R (1982) A calcium-dependent transient outward current in Xenopus laevis oocytes. *Proc R Soc Lond B Biol Sci* 215(1201):491–497.
25. Wagner JA, et al. (1991) Activation of chloride channels in normal and cystic fibrosis airway epithelial cells by multifunctional calcium/calmodulin-dependent protein kinase. *Nature* 349(6312):793–796.
26. Kleene SJ, Gesteland RC (1991) Calcium-activated chloride conductance in frog olfactory cilia. *J Neurosci* 11(11):3624–3629.
27. Caputo A, et al. (2008) TMEM16A, a membrane protein associated with calcium-dependent chloride channel activity. *Science* 322(5901):590–594.
28. Hartzell C, Putzier I, Arreola J (2005) Calcium-activated chloride channels. *Annu Rev Physiol* 67:719–758.
29. Yang YD, et al. (2008) TMEM16A confers receptor-activated calcium-dependent chloride conductance. *Nature* 455(7217):1210–1215.
30. Schroeder BC, Cheng T, Jan YN, Jan LY (2008) Expression cloning of TMEM16A as a calcium-activated chloride channel subunit. *Cell* 134(6):1019–1029.
31. Scudieri P, Sondo E, Ferrera L, Galietta LJ (2012) The anoctamin family: TMEM16A and TMEM16B as calcium-activated chloride channels. *Exp Physiol* 97(2):177–183.
32. Ayoub C, et al. (2010) ANO1 amplification and expression in HNSCC with a high propensity for future distant metastasis and its functions in HNSCC cell lines. *Br J Cancer* 103(5):715–726.
33. Huang X, Godfrey TE, Gooding WE, McCarty KS, Jr, Gollin SM (2006) Comprehensive genome and transcriptome analysis of the 11q13 amplicon in human oral cancer and synteny to the 7F5 amplicon in murine oral carcinoma. *Genes Chromosomes Cancer* 45(11):1058–1069.
34. Rohrbough J, Spitzer NC (1996) Regulation of intracellular Cl- levels by Na(+)-dependent Cl- cotransport distinguishes depolarizing from hyperpolarizing GABAA receptor-mediated responses in spinal neurons. *J Neurosci* 16(1):82–91.
35. Sipilä ST, Schuchmann S, Voipio J, Yamada J, Kaila K (2006) The cation-chloride cotransporter NKCC1 promotes sharp waves in the neonatal rat hippocampus. *J Physiol* 573(Pt 3):765–773.
36. Yamada J, et al. (2004) Cl- uptake promoting depolarizing GABA actions in immature rat neocortical neurones is mediated by NKCC1. *J Physiol* 557(Pt 3):829–841.
37. Owens DF, Boyce LH, Davis MB, Kriegstein AR (1996) Excitatory GABA responses in embryonic and neonatal cortical slices demonstrated by gramicidin perforated-patch recordings and calcium imaging. *J Neurosci* 16(20):6414–6423.
38. Reichling DB, Kyrozis A, Wang J, MacDermott AB (1994) Mechanisms of GABA and glycine depolarization-induced calcium transients in rat dorsal horn neurons. *J Physiol* 476(3):411–421.
39. Eilers J, Plant TD, Marandi N, Konnerth A (2001) GABA-mediated Ca2+ signalling in developing rat cerebellar Purkinje neurones. *J Physiol* 536(Pt 2):429–437.
40. Milenkovic I, Rubsamen R (2011) Development of the chloride homeostasis in the auditory brainstem. *Physiological research* 60(Suppl 1):S15–S27.
41. Baccei ML, Fitzgerald M (2004) Development of GABAergic and glycinergic transmission in the neonatal rat dorsal horn. *J Neurosci* 24(20):4749–4757.
42. Tyzio R, et al. (2006) Maternal oxytocin triggers a transient inhibitory switch in GABA signaling in the fetal brain during delivery. *Science* 314(5806):1788–1792.
43. Belenky MA, Yarom Y, Pickard GE (2008) Heterogeneous expression of gamma-aminobutyric acid and gamma-aminobutyric acid-associated receptors and transporters in the rat suprachiasmatic nucleus. *J Comp Neurol* 506(4):708–732.
44. Vardi N, Zhang LL, Payne JA, Sterling P (2000) Evidence that different cation chloride cotransporters in retinal neurons allow opposite responses to GABA. *J Neurosci* 20(20):7657–7663.
45. Ulrich D, Huguenard JR (1997) Nucleus-specific chloride homeostasis in rat thalamus. *J Neurosci* 17(7):2348–2354.
46. Becker M, Nothwang HG, Friauf E (2003) Differential expression pattern of chloride transporters NCC, NKCC2, KCC1, KCC3, KCC4, and AE3 in the developing rat auditory brainstem. *Cell Tissue Res* 312(2):155–165.
47. Kakazu Y, Akaike N, Komiyama S, Nabekura J (1999) Regulation of intracellular chloride by cotransporters in developing lateral superior olive neurons. *J Neurosci* 19(8):2843–2851.
48. Born DE, Rubel EW (1985) Afferent influences on brain stem auditory nuclei of the chicken: neuron number and size following cochlea removal. *J Comp Neurol* 231(4): 435–445.
49. Saunders JC, Adler HJ, Cohen YE, Smullen S, Kazahaya K (1998) Morphometric changes in the chick nucleus magnocellularis following acoustic overstimulation. *J Comp Neurol* 390(3):412–426.
50. Verkman AS (1990) Development and biological applications of chloride-sensitive fluorescent indicators. *Am J Physiol* 259(3 Pt 1):C375–C388.
51. Rodriguez-Contreras A, Yamoah EN (2001) Direct measurement of single-channel Ca(2+) currents in bullfrog hair cells reveals two distinct channel subtypes. *J Physiol* 534(Pt 3):669–689.